NANOMATERIALS

Biphenylene network: A nonbenzenoid carbon allotrope

Qitang Fan[1]†, Linghao Yan[2]†, Matthias W. Tripp[1], Ondřej Krejčí[2], Stavrina Dimosthenous[2], Stefan R. Kachel[1], Mengyi Chen[1], Adam S. Foster[2,3], Ulrich Koert[1], Peter Liljeroth[2]*, J. Michael Gottfried[1]*

The quest for planar sp^2-hybridized carbon allotropes other than graphene, such as graphenylene and biphenylene networks, has stimulated substantial research efforts because of the materials' predicted mechanical, electronic, and transport properties. However, their syntheses remain challenging given the lack of reliable protocols for generating nonhexagonal rings during the in-plane tiling of carbon atoms. We report the bottom-up growth of an ultraflat biphenylene network with periodically arranged four-, six-, and eight-membered rings of sp^2-hybridized carbon atoms through an on-surface interpolymer dehydrofluorination (HF-zipping) reaction. The characterization of this biphenylene network by scanning probe methods reveals that it is metallic rather than a dielectric. We expect the interpolymer HF-zipping method to complement the toolbox for the synthesis of other nonbenzenoid carbon allotropes.

The synthesis of fullerenes (*1*), carbon nanotubes (*2*), graphene (*3*), and cyclo[18]carbon (*4*) from customized molecular precursors has initiated the era of designer carbon allotropes built from sp, sp^2, and sp^3-hybridized carbon atoms (*5*). Although numerous sp^2-hybridized planar carbon allotropes such as graphene (*6*), pentaheptite (*7*), and biphenylene network (*8*) were proposed (Fig. 1A), only graphene has been realized as a purely hexagonal net (*3*). Progress in the synthesis of other planar three-coordinate carbon nets (*6*) with nonhexagons such as four-, five-, seven-, and eight-membered rings has been very limited. Recently, expanding on the highly successful bottom-up synthesis of benzenoid graphene-related nanostructures (*9*–*13*), several nonbenzenoid nanographenes (*14*–*17*) and nanoribbons (*18*–*20*) with embedded nonhexagonal rings were reported.

Nonetheless, these carbon nanostructures only exhibit repeating nonhexagonal motifs along one dimension, which has hampered the study of the properties of planar nonbenzenoid carbon allotropes. For instance, the successful synthesis and characterization of biphenylene polymer chains cannot serve to clarify the theoretical debate on whether a biphenylene network is dielectric (*21*) or metallic (*22*, *23*). Attempts to add nonhexagonal carbon rings along the second dimension through hierarchical polymerization of nonbenzenoid molecules were of limited success. For example, the lateral fusion of polyazulene chains yielded only small segments of phagraphene (*24*), a planar carbon net with five-, six-, and seven-membered rings, because the orientation of the azulene moieties could not be controlled (*25*). Similarly, efforts toward the synthesis of a biphenylene network (BPN, Fig. 1B) through sequential deiodinative and debrominative coupling of 1,4,5,8-tetraiodo-2,3,6,7-tetrabromobiphenylene (TTBP, Fig. 1B) failed at the initial polymerization step (*26*).

Here, we demonstrate an alternative approach in which the nonbenzenoid structural elements were not contained in the precursor but were formed during the lateral dehydrofluorination (HF-zipping) fusion of benzenoid polyphenylene chains. As shown in Fig. 1C, 4,4″-dibromo-2,2′,2″,5,5′,5″-hexafluoro-1,1′:4′,1″-terphenyl (DHTP) first polymerized through debrominative coupling (*27*) on a Au(111) surface and formed well-aligned assemblies of poly(2,5-difluoro-*para*-phenylene) (PFPP) chains. In a second step, these chains underwent C-C coupling by HF-zipping (*28*–*31*) to form a biphenylene network. The interchain HF-zipping allowed C-C bond formation exclusively between a C-F and a C-H moiety (Fig. 1C, cyan ovals) but not between two C-H or two C-F moieties. As a result, four- and eight-membered rings formed selectively between the chains. Adequately positioned C-F moieties were essential for the formation of the nonbenzenoid structure. In their absence, such as in the case of plain poly(*para*-phenylene) chains, dehydrogenative C-C coupling led to the formation of six-membered rings and thus to regular graphene (*32*, *33*).

The monomer DHTP was synthesized in solution through a two-step sequence (see supplementary materials) and then vapor-deposited in ultrahigh vacuum onto a clean Au(111) surface held at 300 K. Related scanning tunneling microscopy (STM) images are shown in fig. S1. Subsequent annealing to 500 K induced the formation of PFPP chains by debrominative C-C coupling. An ordered island of well-aligned PFPP chains (Fig. 2A) exhibited a pronounced zigzag appearance in the zoom-in STM image in Fig. 2D. The periodicity of 8.8 ± 0.2 Å along the chain arose from alternating up-down tilting of the 2,5-difluoro-*para*-phenylene (FPP) units, as illustrated by the overlaid chemical structure in Fig. 2D. This model was confirmed by the noncontact atomic force microscopy (nc-AFM) image in fig. S2B.

The aligned PFPP chains fused laterally through HF-zipping to form a biphenylene network during annealing to 680 K, as shown by the STM image in Fig. 2B. This condensation reaction resulted in considerable lateral contraction. The high-resolution nc-AFM images (Fig. 2, E and F) of the regions marked by the white rectangles in Fig. 2B revealed armchair-edged biphenylene ribbons (BPRs) with widths of 12 and 18 carbon atoms (12-BPR and 18-BPR). These BPRs have alternating H/F edge termination rather than pure H termination, as illustrated by the chemical structure in Fig. 2E and confirmed by the simulated AFM images in figs. S3 and S4. The widest ribbon we observed (21-BPR) was achieved by further annealing the sample in Fig. 2B to 700 K (Fig. 2C).

The selectivity for biphenylene network formation is related to the two-dimensional (2D) chirality of the PFPP chains. Only HF-zipping between chains of identical handedness led to four- and eight-membered rings (4-8 type fusion; Fig. 2D). Otherwise, six-membered rings formed (6-6 type fusion; Fig. 2D), resulting in the formation of an armchair-edged graphene nanoribbon (6-AGNR) with the normal benzenoid topology (fig. S6). The 4-8 type fusion was overall favored [2.4 (±0.3):1 over the 6-6 type; see supplementary text and fig. S8 for yield analysis] because each PFPP domain consisted mainly of chains with identical handedness, such as the R_a handedness in Fig. 2D (see also fig. S5). Therefore, the aggregation of the PFPP chains in almost homochiral domains was essential for the formation of a biphenylene network. Furthermore, sufficient length of the PFPP chains is a prerequisite for the formation of wide BPRs (see supplementary text).

The reaction progress was monitored by x-ray photoelectron spectroscopy (XPS) (Fig. 2G) and temperature-programmed desorption (TPD) mass spectrometry (Fig. 2H). For as-deposited DHTP on Au(111) at 300 K (Fig. 2G, 300 K), the F1s (686.8 eV) and $Br3p_{3/2}$ (183.5 eV) binding energies were typical for C-F and C-Br groups (*28*, *34*) and confirmed that carbon-halogen bonds were intact. The C1s signal could be consistently deconvoluted into four components attributed to C-F (pink), C-Br (yellow), C-H (cyan), and C-C (blue) with 1:3:3:2

[1]Department of Chemistry, Philipps-Universität Marburg, 35032 Marburg, Germany. [2]Department of Applied Physics, Aalto University, FI-00076 Aalto, Finland. [3]Nano Life Science Institute (WPI-NanoLSI), Kanazawa University, Kakuma-machi, 920-1192 Kanazawa, Japan.
†These authors contributed equally to this work.
*Corresponding author. Email: peter.liljeroth@aalto.fi (P.L.); michael.gottfried@chemie.uni-marburg.de (J.M.G.)

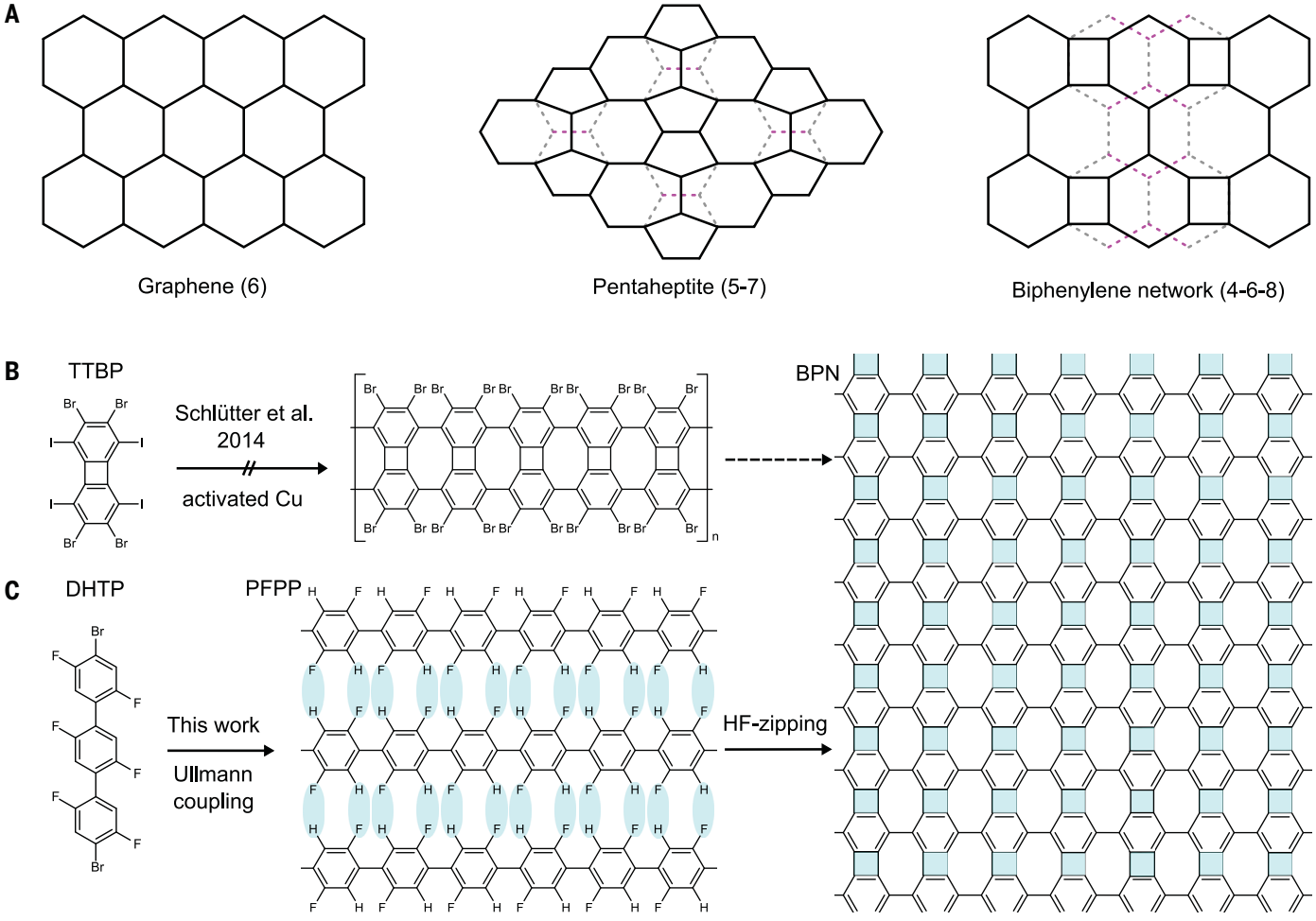

Fig. 1. Synthetic strategies toward the planar nonbenzenoid biphenylene network (BPN). (**A**) Lattice structures of three planar carbon allotropes: graphene, carbon pentaheptite (5-7), and biphenylene network (4-6-8). The latter two formally result from graphene by reorganization of bonds (magenta dotted lines). (**B**) Previous attempts toward the synthesis of BPN from the TTBP monomer. (**C**) DHTP monomer forming BPN by a two-step sequence consisting of linear polymerization followed by interchain HF-zipping.

intensity ratios, in agreement with the composition of DHTP. XPS also confirmed the formation of PFPP chains at 500 K: Lowering of the Br3p$_{3/2}$ binding energy by 2.1 eV indicates C-Br bond dissociation (*34*), and the C1s signal could be deconvoluted into three components (1:1:1) representing C-F, C-H, and C-C bonds (Fig. 2G, 500 K), in agreement with the chemical structure of the chains. We attributed the slight overall shifts (–0.3 eV) of C1s and F1s signals to a work-function change (*35*), whereas their attenuation (35% less) was caused by partial desorption of DHTP, as confirmed by the TPD signal of DHTP in Fig. 2H.

The gradual attenuation of the F1s and C-F–related C1s signals upon further annealing (Fig. 2G, 650 K and 700 K) was indicative of partial removal of fluorine from the C-F groups by HF-zipping. The corresponding TPD trace confirmed HF release above 600 K (Fig. 2H and Fig. S9). Note that the C1s spectra at 650 K and 700 K showed a component at 283.4 eV, labeled C-Au, which we attributed to benzyne intermediates bonding to the surface after removal of H/F pairs in PFPP chains (fig. S11). This component decreased from 650 to 700 K because of the progressive fusion of the PFPP chains. Therefore, we tentatively propose the coexistence of HF-zipping (major reaction pathway) and the benzyne-based mechanism (minor reaction pathway) for the lateral fusion of PFPP chains (see supplementary text and fig. S10).

We systematically characterized BPRs of different widths with scanning tunneling spectroscopy and density functional theory (DFT) calculations. Figure 3A shows the normalized differential conductance (dI/dV) spectra of six different BPRs with widths from 6 to 21 carbon atoms. The spectra were taken at the positions marked by the colored dots in the AFM images on the left sides of Fig. 3, B to G. The narrower BPRs (6-BPR to 12-BPR) showed distinct valence band (VB) and conduction band (CB) onsets (see also additional dI/dV spectra and maps in figs. S13 and S14). Detecting the resonances in the dI/dV spectra corresponding to the band onsets in the wider BPRs (15-BPR to 21-BPR) was more difficult because of the narrow gaps and extra features around zero bias potentially arising from the Au(111) surface state.

We used dI/dV maps (Figs. 3, B to G, middle and right panels, Exp. column) to identity which features in the dI/dV spectra corresponded to states with similar symmetry relative to the VB and CB of the narrower BPRs (see also additional dI/dV spectra and maps in figs. S15 to S17). These features matched the simulated dI/dV maps of the VB and CB onsets (Fig. 3, B to G, middle and right panels, Theory column). For 21-BPR, we could detect orbital features in the dI/dV maps (Fig. 3G and fig. S17B) at all bias

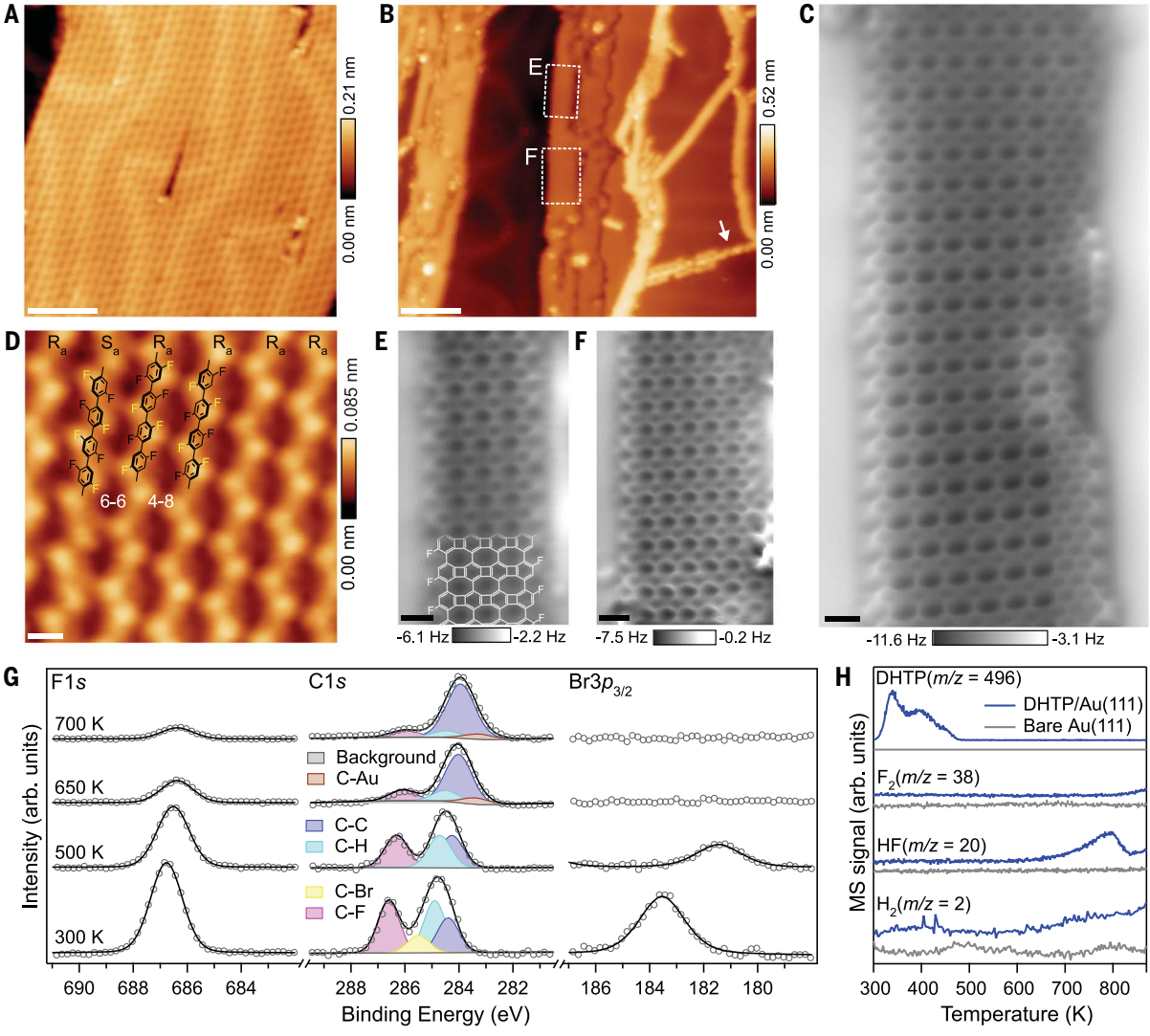

Fig. 2. Formation of biphenylene network by two-step polymerization of DHTP. (**A** and **B**) Overview STM images taken after deposition of DHTP onto Au(111) at 300 K followed by post-annealing to 500 K (A) and 680 K (B). The white arrow in (B) marks a remaining PFPP chain for comparison. (**C**) nc-AFM image of a wide biphenylene ribbon (BPR) obtained by further annealing of the sample in (B) to 700 K. Note that the BPR is jointed with regular graphene at the right side due to minor parasitic 6-6 type fusion. (**D**) Zoom-in STM image of the PFPP chains in (A) overlaid with chemical structures; 2D enantiomers labeled with R_a and S_a. (**E** and **F**) Zoom-in nc-AFM images of the BPRs outlined by the white rectangles in panel (B). The image in (E) is overlaid with the chemical structure. Scale bars, 5 nm [(A) and (B)], 0.5 nm [(C) to (F)]. (**G**) XPS spectra for the indicated core levels and annealing temperatures. (**H**) Mass spectrometer signals for the indicated *m/z* values recorded during controlled heating (1 K/s) of bare and monolayer DHTP-covered Au(111).

voltages, indicating the closing of the gap corresponding to metallic electronic structure. In addition, as assessed by comparison with simulation, the zero-bias dI/dV map corresponded to a mixture of the VB and CB features (arising from states at different momenta; see fig. S19 for calculated band structures), again consistent with the metallic response.

The bandgap evolution of the BPRs with different widths is summarized in Fig. 4. The measured gaps are overall somewhat larger than the values predicted by DFT at the HSE06 level, but the trend of decreasing bandgaps with increasing widths of the BPRs (Fig. 4, magenta line) agreed well with calculations (black line). This decrease was much steeper than that for the corresponding AGNR series reported previously (Fig. 4, blue line) (*33*, *36*). In contrast to the benzenoid AGNRs, the bandgap of the nonbenzenoid BPRs closed completely between 18-BPR and 21-BPR. According to the DFT calculations, the edge termination has no substantial influence on the bandgaps of the BPRs (fig. S19). This result was also consistent with the predicted bandgaps of pure H-terminated BPRs in previous work (*22*) (fig. S20). The rapid decrease of the measured gaps (from 2.35 to 0 eV) of biphenylene networks with increasing sizes provided strong evidence that this material had metallic character, rather than being dielectric with a gap of 2 eV, as was reported in a previous theoretical study (*21*).

Our interpolymer HF-zipping technique for the formation of rings with nonbenzenoid topology in a periodic arrangement paves the way for the exploration of new planar sp^2 carbon allotropes and their properties. Further synthesis progress will focus on increasing yield and selectivity, where the on-surface approach can offer distinct advantages over solution-based reactions (*37*). The HF-zipping reaction is also expected to work on metal-oxide surfaces (*28*, *30*), offering decoupling from the metallic substrate. Further direct

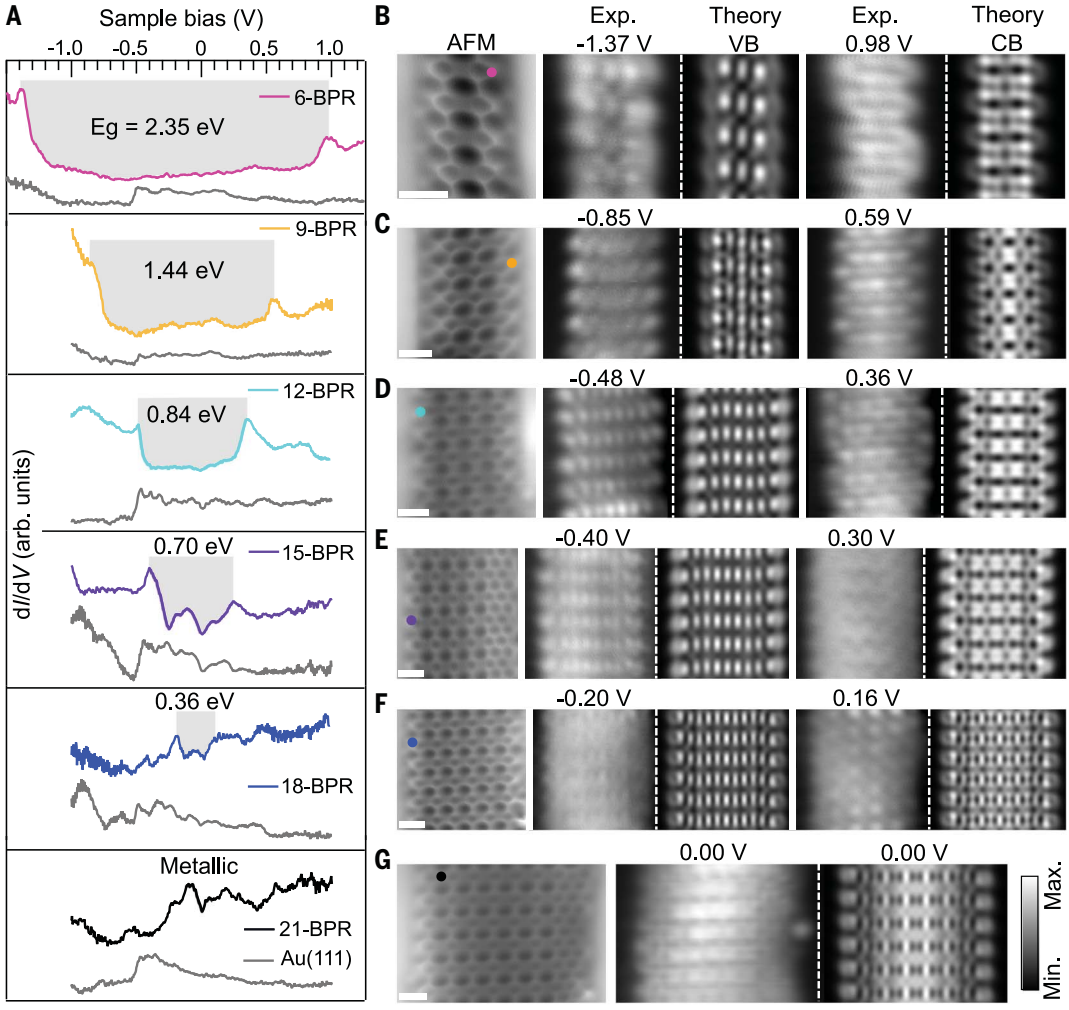

Fig. 3. Electronic properties of BPRs with different widths. (**A**) Differential conductance (d*I*/d*V*) spectra (colored curves) taken at the positions marked with corresponding colored dots in the leftmost panels of (B) to (G). The gray curves are reference d*I*/d*V* spectra taken at clean Au(111). The shaded regions denote the bandgaps between the peaks related to VB and CB onsets. (**B** to **G**) nc-AFM images, experimental and simulated d*I*/d*V* maps at the VB and CB onsets of the 6-BPR (B), 9-BPR (C), 12-BPR (D), 15-BPR (E), 18-BPR (F), and 21-BPR (G). These nc-AFM images are cutouts of the nc-AFM images in Fig. 2, C, E, and F and fig. S12, C to E. The simulated d*I*/d*V* maps are consistent with fluorine substituents at the edges (see fig. S18 for a detailed comparison), in agreement with the AFM images. All scale bars, 0.5 nm. The gray scale for all d*I*/d*V* maps is displayed to the right of (G). All d*I*/d*V* spectra and maps were recorded with CO-functionalized tips.

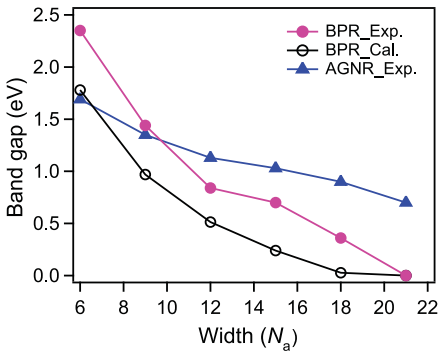

Fig. 4. Bandgaps of BPRs and AGNRs. Comparison between experimental (BPR_Exp.) and calculated (BPR_Cal.) bandgaps of BPRs with AGNRs (AGNR_Exp.) of the same width, as given by the number of carbon atoms, N_a. The AGNR values are adapted from (*33*) on Au(111) and (*36*) on monolayer gold silicide on Au(111).

potential for applications arises from transfer to other substrates or media. For instance, nonbenzenoid 2D carbon allotropes with large rings (>6 members) may represent superior anode materials in lithium-ion batteries because of their predicted larger lithium storage capacity relative to graphene (*38*). The revealed metallicity of the biphenylene network also makes it a candidate for conducting wires in future carbon-based circuitry.

REFERENCES AND NOTES

1. H. W. Kroto, J. R. Heath, S. C. O'Brien, R. F. Curl, R. E. Smalley, *Nature* **318**, 162–163 (1985).
2. S. Iijima, T. Ichihashi, *Nature* **363**, 603–605 (1993).
3. K. S. Novoselov *et al.*, *Science* **306**, 666–669 (2004).
4. K. Kaiser *et al.*, *Science* **365**, 1299–1301 (2019).
5. A. Hirsch, *Nat. Mater.* **9**, 868–871 (2010).
6. A. T. Balaban, *Comput. Math. Appl.* **17**, 397–416 (1989).
7. V. H. Crespi, L. X. Benedict, M. L. Cohen, S. G. Louie, *Phys. Rev. B* **53**, R13303–R13305 (1996).
8. A. T. Balaban, C. C. Rentia, E. Ciupitu, *Rev. Roum. Chim.* **13**, 231–247 (1968).
9. J. Cai *et al.*, *Nature* **466**, 470–473 (2010).
10. D. J. Rizzo *et al.*, *Nature* **560**, 204–208 (2018).
11. P. Ruffieux *et al.*, *Nature* **531**, 489–492 (2016).
12. L. Yan, P. Liljeroth, *Adv. Phys. X* **4**, 1651672 (2019).
13. Z. Chen, A. Narita, K. Müllen, *Adv. Mater.* **32**, e2001893 (2020).
14. S. Mishra *et al.*, *Nat. Commun.* **9**, 1714 (2018).
15. J. Liu *et al.*, *J. Am. Chem. Soc.* **141**, 12011–12020 (2019).
16. J. Hieulle *et al.*, *Nano Lett.* **18**, 418–423 (2018).
17. I. C.-Y. Hou *et al.*, *J. Am. Chem. Soc.* **142**, 10291–10296 (2020).
18. M. Liu *et al.*, *Nat. Commun.* **8**, 14924 (2017).
19. C. Sánchez-Sánchez *et al.*, *Chem. Eur. J.* **25**, 12074–12082 (2019).
20. J. I. Urgel *et al.*, *Angew. Chem. Int. Ed.* **59**, 13281–13287 (2020).
21. N. Tyutyulkov, F. Dietz, K. Müllen, M. Baumgarten, *Chem. Phys. Lett.* **272**, 111–114 (1997).
22. M. A. Hudspeth, B. W. Whitman, V. Barone, J. E. Peralta, *ACS Nano* **4**, 4565–4570 (2010).
23. N. N. Karaush, G. V. Baryshnikov, B. F. Minaev, *Chem. Phys. Lett.* **612**, 229–233 (2014).
24. Z. Wang *et al.*, *Nano Lett.* **15**, 6182–6186 (2015).
25. Q. Fan *et al.*, *J. Am. Chem. Soc.* **141**, 17713–17720 (2019).
26. F. Schlütter, T. Nishiuchi, V. Enkelmann, K. Müllen, *Angew. Chem. Int. Ed.* **53**, 1538–1542 (2014).
27. W. Wang, X. Shi, S. Wang, M. A. Van Hove, N. Lin, *J. Am. Chem. Soc.* **133**, 13264–13267 (2011).
28. M. Kolmer *et al.*, *Science* **363**, 57–60 (2019).
29. A.-K. Steiner, K. Y. Amsharov, *Angew. Chem. Int. Ed.* **56**, 14732–14736 (2017).
30. M. Kolmer *et al.*, *Science* **369**, 571–575 (2020).
31. K. Y. Amsharov, P. Merz, *J. Org. Chem.* **77**, 5445–5448 (2012).
32. A. Basagni *et al.*, *J. Am. Chem. Soc.* **137**, 1802–1808 (2015).
33. N. Merino-Díez *et al.*, *ACS Nano* **11**, 11661–11668 (2017).
34. D. Han *et al.*, *J. Phys. Chem. C* **124**, 5248–5256 (2020).
35. M. Chen *et al.*, *J. Phys. Chem. C* **118**, 6820–6830 (2014).
36. O. Deniz *et al.*, *Nano Lett.* **17**, 2197–2203 (2017).
37. S. Clair, D. G. de Oteyza, *Chem. Rev.* **119**, 4717–4776 (2019).
38. A. Lherbier *et al.*, *Phys. Rev. Mater.* **2**, 085408 (2018).

ACKNOWLEDGMENTS

This research made use of the Aalto Nanomicroscopy Center (Aalto NMC) facilities. Computing resources from the Aalto Science-IT Project and CSC, Helsinki, are gratefully acknowledged. **Funding:** Supported by the Deutsche Forschungsgemeinschaft through projects 223848855-SFB1083 and GO1812/2-1; the State of Hessen (LOEWE Focus Group PriOSS); the European Research Council (ERC-2017-AdG no. 788185); the Academy of Finland (Academy professor funding nos. 318995 and 320555 and project nos. 311012 and 314882); an Alexander von Humboldt Foundation

research fellowship for postdoctoral researchers (Q.F.); the European Union's Horizon 2020 research and innovation program (Marie Skłodowska-Curie Actions Individual Fellowship nos. 839242 and 845060) (L.Y. and O.K.); and the World Premier International Research Center Initiative (WPI), MEXT, Japan (A.S.F.). **Author contributions:** J.M.G., P.L., and U.K. conceived and supervised the experiments; Q.F., L.Y., and M.C. developed the on-surface synthesis protocols and did the STM/AFM measurements and the spectroscopic analysis; M.W.T. synthesized the precursor monomers; S.R.K. did the TPD experiments; O.K. and S.D. performed the simulations under the supervision of A.S.F.; Q.F., L.Y., O.K., and S.D. made the figures; and Q.F., L.Y., P.L., and J.M.G. cowrote the paper. All authors discussed the results and commented on the manuscript at all stages. **Competing interests:** The authors declare no competing financial interests. **Data and materials availability:** All data are available in the main text or the supplementary materials. Data and metadata for all simulations are openly available at doi.org/10.5281/zenodo.4740196 under a CC-BY 4.0 license.

SUPPLEMENTARY MATERIALS

science.sciencemag.org/content/372/6544/852/suppl/DC1
Materials and Methods
Supplementary Text
Figs. S1 to S24
References (*39*–*51*)

6 January 2021; accepted 14 April 2021
10.1126/science.abg4509

Biphenylene network: A nonbenzenoid carbon allotrope

Qitang Fan, Linghao Yan, Matthias W. Tripp, Ondrej Krejcí, Stavrina Dimosthenous, Stefan R. Kachel, Mengyi Chen, Adam S. Foster, Ulrich Koert, Peter Liljeroth and J. Michael Gottfried

Science **372** (6544), 852-856.
DOI: 10.1126/science.abg4509

Biphenylene carbon sheets

Although graphene forms two-dimensional carbon sheets, other arrangements of carbon rings could also assemble as flat sheers. Fan *et al.* synthesized an ultraflat biphenylene carbon sheet consisting of sp^2-hybridized carbon atoms forming four-, six-, and eight-membered rings on a gold surface. An adsorbed halogenated terphenyl molecule undergoes a two-step interpolymer dehydrofluorination polymerization that creates the four- and eight-membered rings through carbon–carbon bond formation. Scanning tunneling spectroscopy revealed that this carbon allotrope is metallic.

Science, abg4509, this issue p. 852